Available online at www.sciencedirect.com
ScienceDirect
Journal of Power Sources 175 (2008) 345–352
JOURNAL OF POWER SOURCES
www.elsevier.com/locate/jpowsour

Effects of GDC interlayer on performance of low-temperature SOFCs

Min Yang [a,b], Aiyu Yan [a,b], Min Zhang [a,b], Zhifang Hou [a], Yonglai Dong [a], Mojie Cheng [a,*]

[a] *Dalian Institute of Chemical Physics, Chinese Academy of Sciences, 457 Zhongshan Road, Dalian 116023, PR China*
[b] *Graduate School of the Chinese Academy of Sciences, Beijing 100049, PR China*

Received 18 July 2007; received in revised form 7 September 2007; accepted 10 September 2007
Available online 14 September 2007

Abstract

To bridge the sintering temperature gap between the electrolyte and the cathode, low-temperature anode supported solid oxide fuel cells (SOFCs) with various thickness of electrolyte interlayer were fabricated and investigated. The porous thin interlayer was dip-coated and fired onto the dense $Ce_{0.9}Gd_{0.1}O_{1.95}$ (GDC) electrolyte surface. With humidified hydrogen as the fuel and air as the oxidant, the single cell with a 0.15 μm interlayer achieved the maximum power density (MPD) of 0.9 W cm^{-2} at 600 °C. The higher open circuit voltages (OCVs) (>0.9 V at 600 °C) were obtained in this study. The impedance results showed that the porous interlayer not only improved the interfacial contact between electrolyte and cathode, but also increased electrochemically active surface area. The cathode/electrolyte polarization resistance exhibited minimum when a 0.15 μm interlayer was added. The apparent activation energies derived from the Arrhenius plots of interfacial polarization resistances were about the same when the added interlayer was thinner, which indicated that the reaction mechanism did not change. However, the corresponding values were higher as the thick interlayer was introduced, which could be ascribed to the retarded oxygen ion transfer in the added porous layer. The cell area specific resistance (ASR) obtained by linear fitting *I–V* plot in the region of 0.6–0.7 V was higher than the ohmic resistance tested at OCV condition, and it was potentially attributed to the increased oxygen partial pressure at the anode as well as the contribution from polarization resistance, i.e. polarization of mass transport.

Keywords: Solid oxide fuel cells; $Ce_{0.9}Gd_{0.1}O_{1.95}$; Interfacial modification; Impedance spectroscopy; Open circuit voltage

1. Introduction

In the recent years, a number of investigations on solid oxide fuel cells (SOFCs) have been devoted to reduce the operation temperature. Low-temperature operation implies higher Nernst voltage. It allows the use of cheap stainless steel for the bipolar plates and the balance of the plant, together with the use of compliant high-temperature gaskets rather than rigid glass-based seals. Doped ceria, such as gadolinia doped ceria (GDC) and samaria doped ceria (SDC) are therefore adopted as the electrolyte [1–4], and highly active perovskites, such as $Ba_{0.5}Sr_{0.5}Co_{0.8}Fe_{0.2}O_{3-\delta}$ (BSCF), are used as the cathode materials [5–7].

The recent noticeable development on anode supported SOFC with ceria-based electrolyte is that the high power densities, e.g. 1.010 and 1.329 W cm^{-2}, are obtained at a relatively low temperature of 600 °C [7,8]. However, many obstacles still exist and should be overcome. The main disadvantages of doped $CeO_{2-\delta}$ ceramics are associated with a relatively easy reducibility at low oxygen partial pressures, which accelerated electronic transport and possible mechanical decomposition under large oxygen chemical potential gradients typical of SOFC operation [4,9]. Therefore the open circuit voltages (OCVs) are lower for the internal short circuit and gas leakage of the electrolyte. Some OCV values reported in literatures are summarized in Table 1. All the cells were tested with humidified hydrogen as the fuel and air as the oxidant. From the data in Table 1, it can be seen that the higher OCVs (>0.9 V at 600 °C) are obtained only when the electrolyte is thick or the fuel cell geometric area is small. Nevertheless, for the cells which are more practical, in which the electrolyte thickness is 20–35 μm and the geometric area is 0.25–1.2 cm^2, the OCVs are lower. In addition, the stability of the cell is also negatively affected by the reducibility of the ceria-based ceramics in the anode substrate and electrolyte.

Another problem for the ceria-based electrolyte SOFCs pertains to the cathode/electrolyte interface. Presently, anode-

* Corresponding author. Tel.: +86 411 84379049; fax: +86 411 84379049.
E-mail address: mjcheng@dicp.ac.cn (M. Cheng).

0378-7753/$ – see front matter © 2007 Elsevier B.V. All rights reserved.
doi:10.1016/j.jpowsour.2007.09.019

Table 1
OCVs of single cells with ceria-based electrolyte in literatures

Electrolyte	Cathode	Cell geometric area (cm^2)	OCV (V) at 600 °C	OCV (V) at 500 °C	Refs.
10 μm $Ce_{0.9}Gd_{0.1}O_{1.95}$	$Ba_{0.5}Sr_{0.5}Co_{0.8}Fe_{0.2}O_3$	0.005	0.903	0.984	[8]
10 μm $Sm_{0.2}Ce_{0.8}O_{1.9}$	$Sm_{0.5}Sr_{0.5}CoO_3$-SDC	1.35	0.835	0.873	[10]
20 μm $Sm_{0.15}Ce_{0.85}O_2$	$Ba_{0.5}Sr_{0.5}Co_{0.8}Fe_{0.2}O_3$	-	~0.85	~0.91	[7]
20 μm $Sm_{0.2}Ce_{0.8}O_{1.9}$	$La_{0.6}Sr_{0.4}Co_{0.2}Fe_{0.8}O_3$	0.5	~0.85	~0.9	[11]
18-20 μm $Sm_{0.2}Ce_{0.8}O_{1.9}$	$Sm_{0.5}Sr_{0.5}CoO_3$-SDC	1.33	0.879	0.945	[12]
26 μm $Ce_{0.9}Gd_{0.1}O_{1.95}$	$Sm_{0.5}Sr_{0.5}CoO_3$-SDC	-	~0.83	~0.9	[13]
30 μm $Sm_{0.2}Ce_{0.8}O_{1.9}$	$Sm_{0.5}Sr_{0.5}CoO_3$-SDC	-	~0.86	~0.92	[14]
35 μm $Sm_{0.2}Ce_{0.8}O_{1.9}$	$Sm_{0.5}Sr_{0.5}CoO_3$-SDC	0.25	~0.83	~0.92	[15]
210 μm $Ce_{0.9}Gd_{0.1}O_{1.95}$	$Sm_{0.5}Sr_{0.5}CoO_3$-SDC	0.25	~0.95	~1.0	[16]
400 μm $Sm_{0.2}Ce_{0.8}O_{1.9}$	$Sm_{0.5}Sr_{0.5}CoO_3$-SDC	0.8	~0.91	~0.93	[17]

electrolyte assembly is generally sintered at a temperature over 1350 °C for ensuring a dense electrolyte film. However, the newly developed cathode materials, such as BSCF and $Sm_{0.5}Sr_{0.5}CoO_3$ (SSC), having a low melting temperature and a high reactivity with electrolyte, have to be fired onto the ceria-based electrolyte at a temperature below 1000 °C, even for a composite cathode [11,13,18]. Large sintering temperature gap between the electrolyte and the cathode may result in inferior cathode/electrolyte interfaces and consequently reduce triple-phase boundaries (TPBs). Thus further modification of ceria-based electrolytes is required in order to improve their performance and stability.

The "triple access" of gas, electrons, and oxygen ions to active catalyst sites, namely the TPB, ensures the occurrence of the electrochemical reaction, thus the extension of TPB becomes a determining factor in improving cell performance. TPBs strongly depend on the microstructure and morphology of the electrolyte/electrode interfaces, which in turn are determined by the materials properties and fabrication techniques. At the beginning, the extension of TPBs can be realized by adopting a composite cathode and the fine control of whole cell fabrication process [19,20]. Later, the method of adding an interlayer between the electrolyte and electrode was introduced. Effects of doped ceria interlayer on the cell performance were carried out by Barnett et al. [21–23]. A significant improvement in performance was observed when $(CeO_2)_{0.84}$ $(Y_2O_3)_{0.16}$ (YDC) was introduced at the $La_{0.8}Sr_{0.2}MnO_3$–$(Y_2O_3)_{0.08}(ZrO_2)_{0.92}$ (YSZ)/YSZ and NiO–YSZ/YSZ interfaces, which resulted from the increased surface reactions. Ivers-Tiffée et al. [24,25] had performed the study of enlarging the electrochemical active surface by screen printing individual $(Y_2O_3)_{0.1}(ZrO_2)_{0.9}$ (10YSZ) particles onto $La_{0.75}Sr_{0.2}MnO_3/(Y_2O_3)_{0.08}(ZrO_2)_{0.92}$ (8YSZ) interfaces and developed a finite element model (FEM) for calculating and predicting the electrical performance of a SOFC with a three-dimensional interface between cathode and electrolyte. In a recent work of our group [26], the $La_{0.8}Sr_{0.2}Mn_{1.1}O_3$–YSZ/YSZ interface was modified with a thin layer of $(CeO_2)_{0.01}$ $(Sc_2O_3)_{0.10}$ $(ZrO_2)_{0.89}$ (1Ce10ScZr) electrolyte, in view that 1Ce10ScZr displayed much higher oxygen ionic conductivity than YSZ and the two electrolyte showed good chemical compatibility and similar thermal expansion coefficients. With elicitation of those studies, the addition of a high oxide conductivity and ceria containing interlayer is an effective way for the fine tuning of the interfaces and cell performance.

In order to bridge the sintering gap between the electrolyte and cathode and improve their interface microstructures, a porous GDC interlayer will be introduced with a sintering temperature between those for the electrolyte and cathode in this paper. Low-temperature solid oxide fuel cells with various thickness of GDC interlayer will be fabricated, and the effect of the GDC interlayer on the cell performance will be investigated.

2. Experimental

The home-made $Ba_{0.5}Sr_{0.5}Co_{0.8}Fe_{0.2}O_{3-\delta}$ (BSCF) and $Gd_{0.1}Ce_{0.9}O_{1.95}$ (GDC) powders were synthesized by sol–gel process.

Anode-supported thin electrolyte bilayer assemblies were fabricated using a dual dry-pressing method. The anode, formed from a 50:50 wt.% mixture of NiO and GDC powders was dry-pressed into a pellet, and then an electrolyte powder was distributed on the anode surface and co-pressed with the anode using a uniaxial die-press (Ø25 mm). The resultant bilayer was sintered at 1420 °C for 4 h in air. The GDC electrolyte was coated with the GDC slurry onto its surface, and fired between 1150 and 1350 °C for 2 h in air. The interlayer thickness was calculated from the loading amount and density of GDC on the electrolyte, which was a parameter of loading amount per unit area. The cells with an interlayer thickness of 0.06, 0.15, 0.3, 1.5 and 3 μm were fabricated. A 30 wt.% GDC-containing BSCF cathode (area 0.5 cm^2) was slurry coated on GDC film and fired at 950 °C for 2 h. In this study, the cells modified with the interlayer thickness of 0.06, 0.15, 0.3, 1.5, 3 μm were identified respectively as C1, C2, C3, C4 and C5 thereafter, and the unmodified cell was C0. The GDC thickness was calculated according to the compact film and only denoted the quantity of the GDC slurry.

Two gas chambers were set up by placing the cell between two alumina tubes. Silver meshes were used as current collectors and spring-pressed against the anode and cathode. After the in situ reduction of the NiO anode in flowing H_2 at 700 °C for several hours, the cell performance was measured at 600–500 °C by

changing an external load. The *I–V* characteristic of the anode-supported cell was tested using humidified hydrogen as the fuel (100 ml min^{-1}) and air as the oxidant (200 ml min^{-1}). The impedances were measured typically under open circuit conditions using a Solartron 1287 potentiostat and 1260 frequency response analyzer. The frequency range was from 0.1 to 10 kHz with signal amplitude of 10 mV. After testing, the cell was cooled down to room temperature under flow of humidified hydrogen to the anode and oxygen to the cathode. The microstructures of the cells and the added GDC interlayer were measured by a scanning electron microscope (SEM) equipped with an energy dispersive X-ray (EDX) detector (FEI, QUANTA 200 FEG).

3. Results and discussion

3.1. Microstructure of the electrolyte

Fig. 1 shows SEM micrographs of the cells with a 0.15 μm GDC interlayer and the conventional cell. Since both the cells have the same anode, electrolyte and cathode, their microstructures are about the same, which can be confirmed from the cross section of the cells (Fig. 1a and b). Nickel catalysts are stabilized in the GDC matrix. The thickness of the dense GDC electrolyte is about 20 μm. In the conventional structure cell, a clear interface between the cathode and the electrolyte can be seen (Fig. 1b), suggesting a bad adhesion of the cathode to

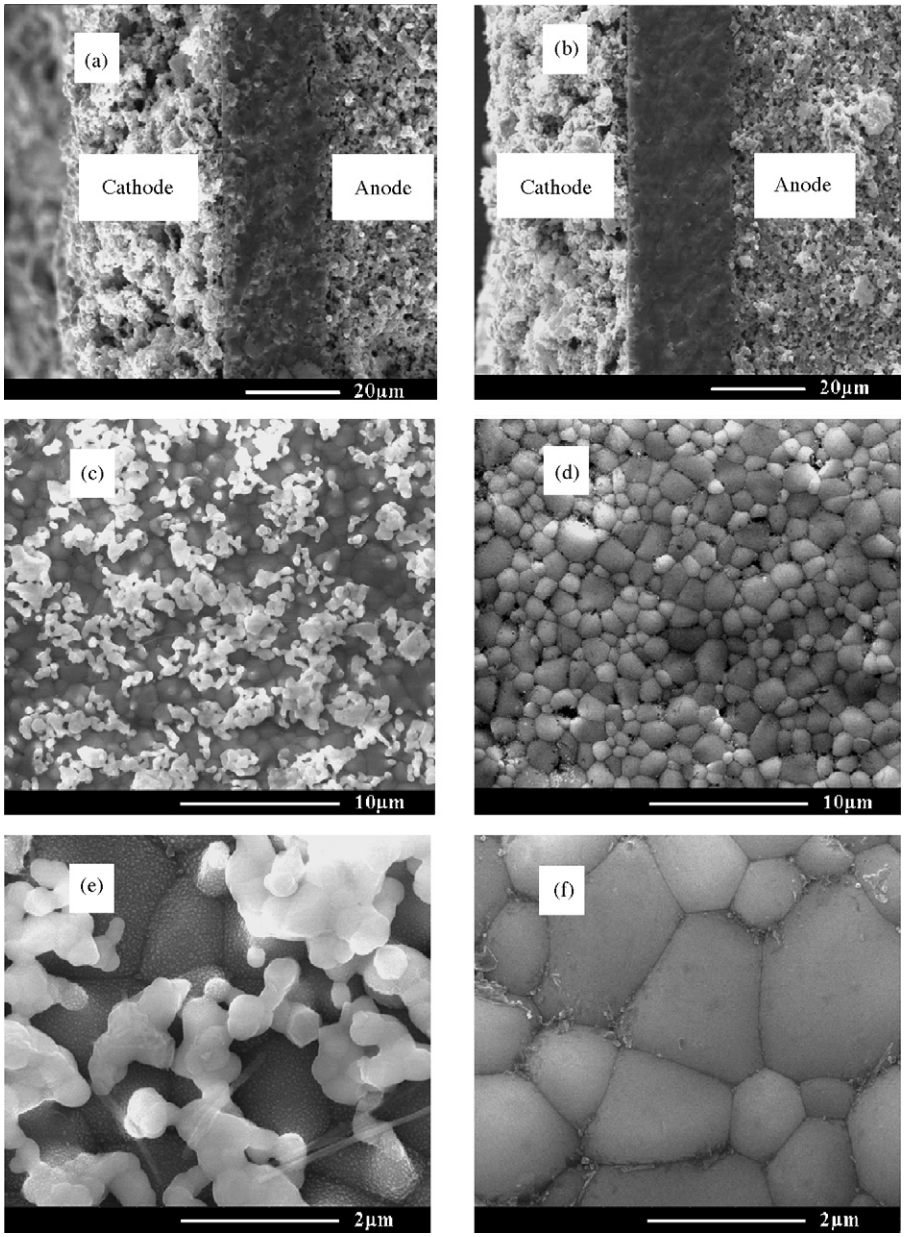

Fig. 1. SEM micrographs of the cross section of the cells (a) with GDC interlayer, (b) without GDC interlayer, and the surface of the cell (c and e) with GDC interlayer, (d and f) without GDC interlayer.

the electrolyte surface. In the modified cell, a 0.15 μm interlayer is invisible because it has been tightly bonded with the dense electrolyte and composite cathode and thus a better electrolyte/cathode interface has been obtained (Fig. 1a). The surface views of these two cells are demonstrated in Fig. 1c–e. It can be seen the uniform electrolyte surface on the unmodified cell (Fig. 1d and f). On the other hand, the electrolyte surface of the modified cell is coated with some small GDC particles (Fig. 1c and e). Because the interlayer is not dense, a portion of the dense electrolyte surface is exposed. As mentioned before, the 0.15 μm thickness only denotes the quantity of the added GDC slurry and cannot be treated as the actual thickness of the interlayer, but the thickness is an effective parameter to quantify the added GDC in this study.

3.2. Electrochemical impedance spectra (EIS) analysis

Fig. 2 shows the impedance spectra of the single cells with different thickness of GDC interlayer at 600 °C, 550 °C and 500 °C, respectively. For the C0, C1, C2 and C3, the impedance spectra at 600 °C show one dominating arc at medium frequency (MF) and a very small arc at high frequency (HF) at 550 °C. However, for the C4 and C5, the arcs at low frequency (LF) become clearly visible at 600 °C and 550 °C. As the temperature lowers to 500 °C, the LF arcs are increased so much that they overlap with the MF arcs, which lead to the reduced peak frequencies and increased magnitude of "MF arcs" compared with those of C0–C3. The LF arcs may reflect the oxygen ion transfer process in this porous thick GDC interlayer, in which the increasing porosity prevents direct grain contact and leads to higher resistance for oxygen vacancy transport [27–30]. The slight increase of HF arcs for C4 and C5 may be ascribed to lower rate of incorporation of the oxygen ions from TPB into GDC lattice. The results above indicate that when the thicker interlayer (1.5 μm or 3 μm in this study) is added at the cathode/electrolyte interface, the oxygen reduction processes can be affected.

Because the electronic conduction in GDC is not negligible under the operation conditions, the polarization resistance (R_p) of the fuel cell based on GDC must be adjusted according to the following Eq. (1) [31], where V_{OC} is the open circuit voltage, E_N is the Nernst potential, R_b represents the intercept of the impedance with the real axis at high frequencies, and R_T corresponds to the intercept at the lowest frequencies.

$$R_p = \frac{R_T - R_b}{(V_{OC})/(E_N)[1 - (R_b)/(R_T)(1 - (V_{OC})/(E_N))]} \quad (1)$$

The added GDC interlayer is desired to extend electrochemical active interfaces per unit volume and thus the interfacial polarization resistance will be reduced. Fig. 3 shows the interfacial polarization resistance (R_p) for single cells as a function of interlayer thickness. It is found that the polarization resistance exhibits the minimum at 0.15 μm thickness of interlayer. However, further increasing GDC interlayer thickness on the cathode/electrolyte surface inhibits the transfer of the oxygen ions from TPBs to the electrolyte as well as their subsequent incorporation into GDC lattice, consequently the polarization

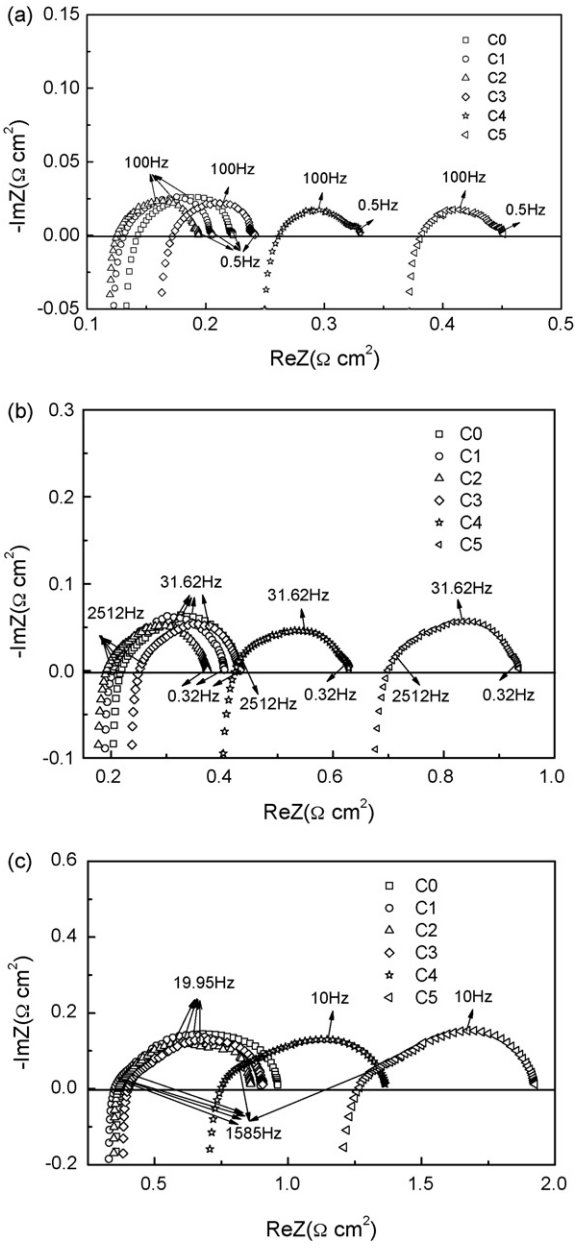

Fig. 2. Electrochemical impedance spectra of the single cells with different thickness of GDC interlayer: measured at (a) 600 °C, (b) 550 °C, (c) 500 °C and under open circuit.

resistance increases. Furthermore, the lower the temperature is, the more evident the variation extent of the polarization resistance is, indicating that at 600 °C the ohmic resistance occupies most of the total resistance whereas at lower temperatures the polarization resistance is overwhelming.

The effect of interlayer thickness on the reaction mechanism can be deduced from Fig. 4, which presents the Arrhenius plots of total interfacial polarization resistance for single cells with different thickness of interlayer. Good linearity of In (R_p^{-1}) versus reciprocal temperature is observed in the investigated temperature range. Adding thinner interlayer (viz. 0.06, 0.15, 0.3 μm) does not change the reaction mechanism of the electrode process, in consideration of the fact that the derived activation

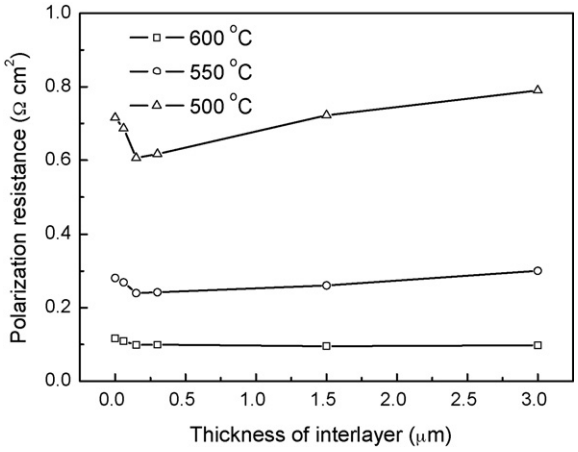

Fig. 3. Interfacial polarization resistance for single cells as function of interlayer thickness.

energies for C0–C3 are 102, 103, 102, 103 kJ mol^{-1}, respectively. These values are in the range for oxygen surface exchange of BSCF [7], which means that this process perhaps dominates the total interfacial polarization resistance of the cell within the range of temperatures under investigation, and the addition of the GDC interlayer does not change the nature of electrochemical process on the cell. The different intercepts of the Arrhenius plots with vertical axis indicate that the interlayer altered pre-exponential coefficient of Arrhenius equation from an increased electrochemical active area.

Inset in Fig. 4 shows the Arrhenius plots of total interfacial polarization resistance for single cells with the thick interlayer (C4, C5). Compared to the thinner interlayer cells (C0–C3), the corresponding activation energies are relatively high. The values of 114 and 117 kJ mol^{-1} have been obtained for C4 and C5, respectively. The impedance spectra depict that the polarization resistance from oxygen anion transfer increases when a thick GDC interlayer is added. The higher activation energy of the cell with a thick interlayer may be from a large contribution from oxygen anion transfer.

Relationship between the specific ohmic resistances of single cells and thickness of the GDC interlayer is illustrated in

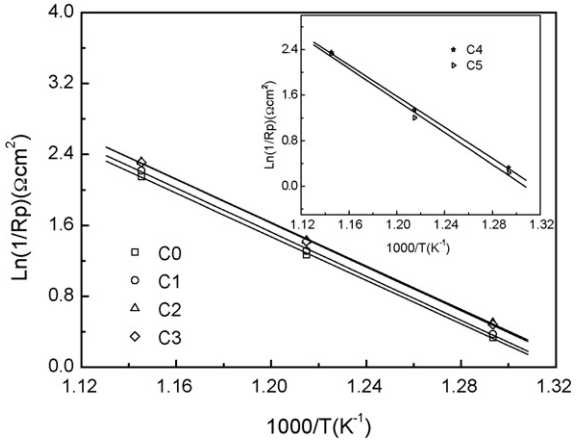

Fig. 4. Arrhenius plots of cathode/electrolyte interfacial resistances for the single cells with different thickness of GDC interlayer.

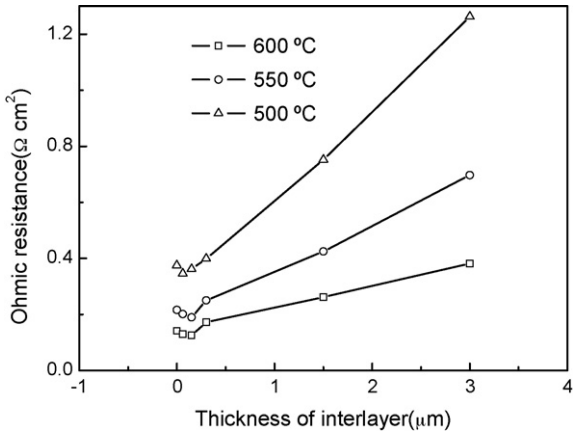

Fig. 5. Relationship between Ohmic resistance of single cells and the thickness of GDC interlayer.

Fig. 5. The minimum specific ohmic resistances of 0.1253 and 0.1901 Ωcm^2 at 600 °C and 550 °C, respectively, are shown on the cell with 0.15 μm GDC interlayer. It is believed the interlayer binders much better with both the electrolyte and the BSCF cathode. As expected, the specific ohmic resistance increases when thicker interlayer is adopted. The specific ohmic resistance at 500 °C behaves similarly as that at 600 °C, except that the minimum occurs on the cell with the interlayer thickness of 0.06 μm.

3.3. Cell performance and open circuit voltage

The cell performances and the corresponding power densities are expressed in Fig. 6 for C0–C5, measured with humidified hydrogen as fuel and air as oxidant at temperatures from 500 to 600 °C. Fig. 7 shows the effect of interlayer thickness on the maximum power density. The optimum performance is obtained when the 0.15 μm thickness interlayer is introduced. The cell performance is determined by the combined effect of the increased active sites and the increased ohmic resistances. When the interlayer thickness is smaller than the optimum, the active sites dominate the cathode performance. Otherwise, the ohmic resistance is the governing factor. Unlike the most adopted 60–65 wt.% NiO in the anode composition [7,8,10,11,16,32], the anode in this study consists of 50 wt.% NiO and 50 wt.% GDC to ensure the dense electrolyte as well as the good stability of the cell. According to Fig. 2a and c, when the cells are operated at 600 °C, significant fractions of the overall cell resistances (63.6%, 63.1%, 64.4%, 71.3%, 78.8%, and 84.6% respectively for C0–C5) are attributed to the ohmic resistances. But when the operation temperature falls off to 500 °C, the ratios of the ohmic resistance to the total lowered, and the corresponding values are reduced to 39.1%, 38.4%, 42.3%, 44.1%, 55.7% and 66.1%. Thus, optimizing the electrode and interface structures to minimize the electrode polarization resistances becomes more important.

The cell area specific resistance (ASR) is obtained by linear fitting *I–V* plots in the region of 0.6–0.7 V. The relationship between the cell ASRs and the thickness of interlayer is illustrated in Fig. 8. Within the temperature region investigated, the cell with 0.15 μm thickness interlayer obtains the minimum

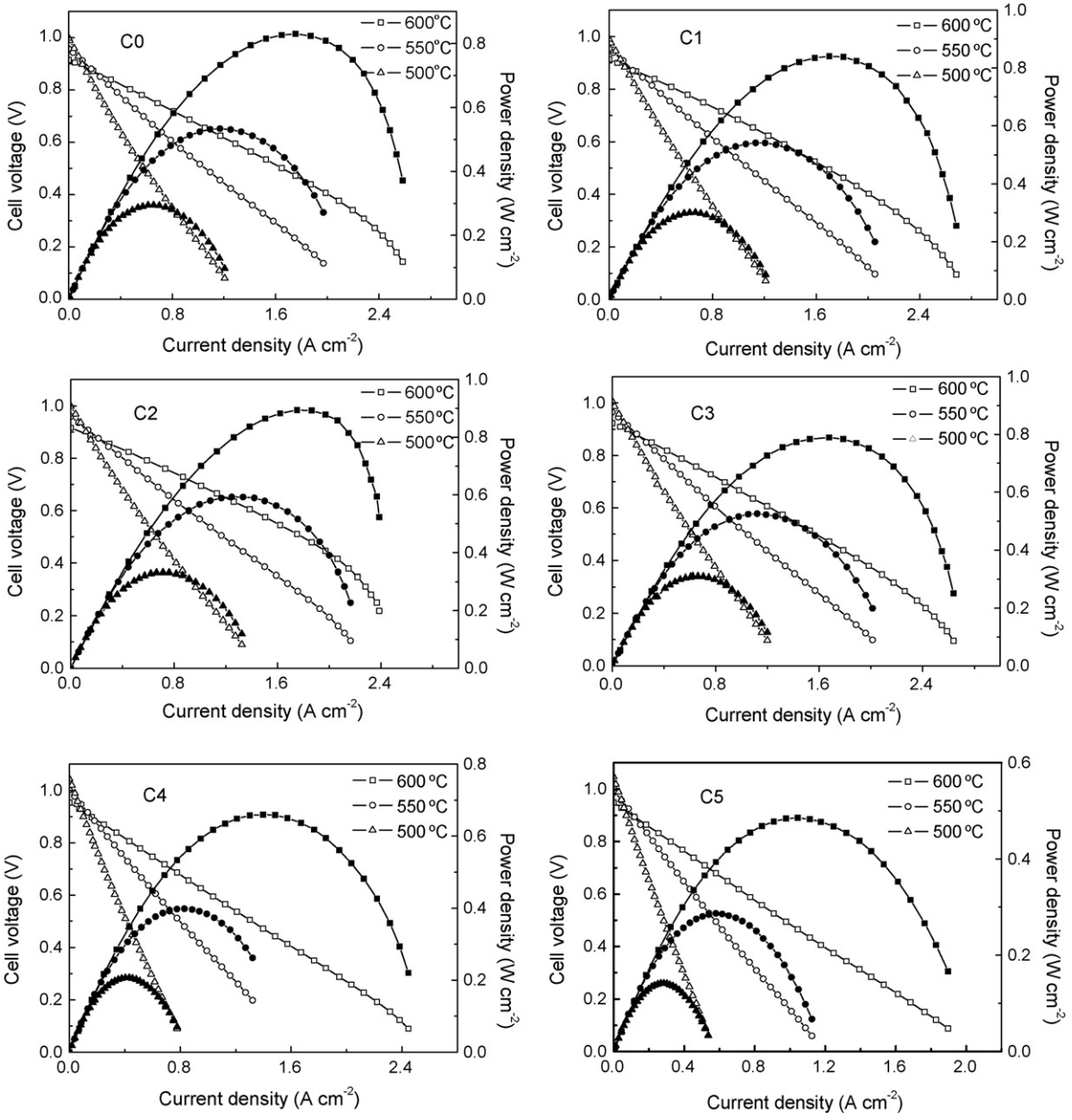

Fig. 6. Cell voltages and power densities as function of current density for the single cells with different thickness of GDC interlayer.

ASR, and this is consistent with the results in Fig. 6. The cell ASRs are higher than the ohmic resistances obtained from the impedance spectra under OCV. The observation can be explained by the well-known fact that the oxygen partial pressure at the anode in the region of 0.6–0.7 V is higher than that at the open circuit conditions, therefore the electronic resistance of the electrolyte is increased, and the cell ASR is higher compared with the ohmic resistance. Another possible reason is that the non-ohmic resistance, including the electrode polarization resistances and the mass transport resistance within the electrodes, may also contribute to the cell ASRs.

As well-known, the OCV can be affected by a lot of factors, such as the operating temperatures, the electrolyte properties, the electrolyte thickness as well as the gas-tightness of the electrolyte, interfacial polarization resistance, electrode nature and oxygen partial pressure in fuel gas etc., especially for ceria-based electrolytes with the mixed ionic and electronic conductivity and the low mechanical properties. Besides, the fuel-cell geometric area would also have an impact on the measurement of OCV value. The smaller the geometric area, the higher the resistance for migration of the charge carriers (oxide ion and electron), and consequently the internal short circuit current will decrease and the OCV will increase. Therefore, the OCV values listed in Table 1 vary from each other. The OCV values obtained in this study are summarized in Table 2, which are in the range of 0.913–0.953 V at 600 °C and 0.989–1.046 V at 500 °C. The higher OCV values in the modified cells of this study can be ascribed to both a gas-tight electrolyte and an increased cathode activity after adding an interlayer. It is obvious that the increase in OCV values upon adding 1.5

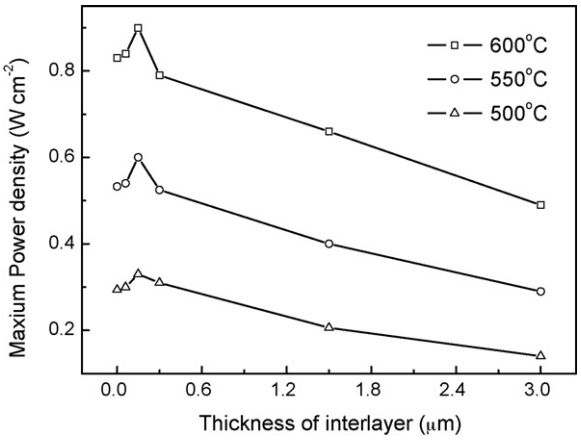

Fig. 7. Effect of interlayer thickness on the maximum power density.

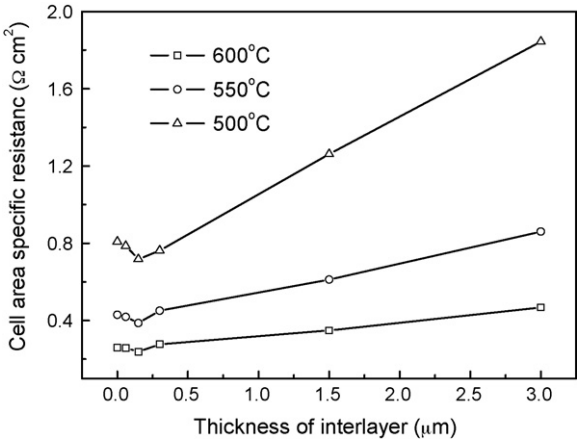

Fig. 8. Relationship between the cell area specific resistances from linear-fitting *I–V* plots in the region of 0.6–0.7 V and the thickness of interlayer.

Table 2
OCVs of single cells with different thickness of interlayer operating at different temperatures

Thickness (μm)		0	0.06	0.15	0.3	1.5	3
OCV (V)	600 °C	0.914	0.913	0.916	0.923	0.953	0.948
	550 °C	0.957	0.953	0.959	0.965	1.001	1.003
	500 °C	0.998	0.989	0.999	1.007	1.044	1.046

and 3 μm thickness of interlayer originates from the retarded electron transport in the porous interlayer.

4. Conclusions

Low-temperature solid oxide fuel cells with various thickness GDC interlayer between the dense GDC electrolyte and BSCF-GDC composite cathode were prepared and investigated. This porous interlayer was advantageous for the interfacial contact between the electrolyte and cathode as well as for extending the TPBs, in which the lowest polarization resistance was obtained when a 0.15 μm interlayer was added. The same activation energies of electrode process for the cells with the thin interlayer suggested that the interlayer extended the TPB without any variation in the electrochemical processes. However, the corresponding values increased when the thick interlayer was introduced, which indicated the change of reaction mechanism. The maximum power density, 0.9 W cm^{-2} at 600 °C, was achieved on the cell with a 0.15 μm interlayer. Higher OCVs (>0.9 V at 600 °C) of these cells indicated a better cell structure, both a gas-tight electrolyte and an increased cathode activity. The cell ASRs were higher when compared with the ohmic resistance measured at the OCV conditions, which may result from the increased oxygen partial pressure at the anode as well as the non-ohmic contribution.

Acknowledgements

The authors gratefully acknowledge financial supports from the Ministry of Science and Technology of China (No. 2004CB719506, 2005CB221404 and 2006AA05Z147) and Europe Commission (SOFC 600).

References

[1] K. Eguchi, T. Setoguchi, T. Inoue, H. Arai, Solid State Ionics 52 (1992) 165–172.
[2] T. Inoue, T. Setoguchi, K. Eguchi, H. Arai, Solid State Ionics 35 (1989) 285–291.
[3] K. Zheng, B.C.H. Steelea, M. Sahibzadab, I.S. Metcalfe, Solid State Ionics 86–88 (1996) 1241–1244.
[4] B.C.H. Steele, Solid State Ionics 129 (2000) 95–110.
[5] Z.P. Shao, W.S. Yang, Y. Cong, H. Dong, J.H. Tong, G.X. Xiong, J. Membr. Sci. 172 (2000) 177–188.
[6] Z.P. Shao, G.X. Xiong, J.H. Tong, H. Dong, W.S. Yang, Sep. Purif. Technol. 25 (2001) 419–429.
[7] Z.P. Shao, S.M. Haile, Nature 431 (2004) 170–173.
[8] Q.L. Liu, K.A. Khor, S.H. Chan, J. Power Sources 161 (2006) 123–128.
[9] A. Atkinson, Solid State Ionics 95 (1997) 249–258.
[10] X.G. Zhang, M. Robertson, C. Deĉes-Petit, W. Qu, O. Kesler, R. Maric, D. Ghosh, J. Power Sources 164 (2007) 668–677.
[11] T. Misono, K. Murata, T. Fukui, J. Chaichanawong, K. Sato, H. Abe, M. Nait, J. Power Sources 157 (2006) 754–757.
[12] X.G. Zhang, M. Robertson, S. Yick, C. Deĉes-Petit, E. Styles, W. Qu, Y.S. Xie, R. Hui, J. Roller, O. Kesler, R. Maric, D. Ghosh, J. Power Sources 160 (2007) 1211–1216.
[13] C.R. Xia, M.L. Liu, Solid State Ionics 144 (2001) 249–255.
[14] C.R. Xia, F.L. Chen, M.L. Liu, Electrochem. Solid-State Lett. 4 (5) (2001) A52–A54.
[15] S.W. Zha, W. Rauch, M.L. Liu, Solid State Ionics 166 (2004) 241–250.
[16] Y.H. Yin, S.Y. Li, C.R. Xia, G.Y. Meng, Electrochim. Acta 51 (2006) 2594–2598.
[17] C.R. Xia, W. Rauch, F.L. Chen, M.L. Liu, Solid State Ionics 149 (2002) 11–19.
[18] Q.S. Zhu, T.G. Jin, Y. Wang, Solid State Ionics 177 (2006) 1199–1204.
[19] T. Kenjo, M. Nishiya, Solid State Ionics 57 (1992) 295–302.
[20] M.J.L. Østergård, C. Clausen, C. Bagger, M. Mogensen, Electrochim. Acta 40 (1995) 1971–1981.
[21] T. Tsai, S.A. Barnett, Solid State Ionics 98 (1997) 191–196.
[22] T. Tsai, S.A. Barnett, J. Electrochem. Soc. 145 (1998) 1696–1701.
[23] E. Perry Murray, T. Tsai, S.A. Barnett, Nature 400 (1999) 649–651.
[24] D. Herbstritt, A. Weber, E. Ivers-Tiffée, J. Eur. Ceram. Soc. 21 (2001) 1813–1816.
[25] A. Weber, E. Ivers-Tiffée, J. Power Sources 127 (2004) 273–283.

[26] Z.W. Wang, M.J. Cheng, Y.L. Dong, M. Zhang, H.M. Zhang, J. Power Sources 156 (2006) 306–310.
[27] T. Suzuki, I. Kosacki, H.U. Anderson, Solid State Ionics 151 (2002) 111–121.
[28] S. Lübke, H.-D. Wiemhöfer, Solid State Ionics 117 (1999) 229–243.
[29] M. Gödickemeier, K. Sasaki, L.J. Gauckler, J. Electrochem. Soc. 144 (1997) 1635–1646.
[30] K. Rajender Reddy, K. Karan, J. Electroceram. 15 (2005) 45–56.
[31] M.L. Liu, H.X. Hu, J. Electrochem. Soc. 143 (1996) L109–L112.
[32] S.W. Zha, A. Moore, H. Abernathy, M.L. Liu, J. Electrochem. Soc. 151 (8) (2004) A1128–A1133.